Journal of Alloys and Compounds 509 (2011) 675–686

Contents lists available at ScienceDirect

Journal of Alloys and Compounds

journal homepage: www.elsevier.com/locate/jallcom

Review

Rare earth–Mg–Ni-based hydrogen storage alloys as negative electrode materials for Ni/MH batteries

Yongfeng Liu, Yanhui Cao, Li Huang, Mingxia Gao, Hongge Pan*

State Key Laboratory of Silicon Materials, Department of Materials Science and Engineering, Zhejiang University, Hangzhou 310027, People's Republic of China

ARTICLE INFO

Article history:
Received 31 May 2010
Received in revised form 17 August 2010
Accepted 25 August 2010
Available online 23 October 2010

Keywords:
Hydrogen storage materials
Metal hydride electrodes
Ni/MH batteries
R–Mg–Ni-based alloys
Electrochemical reactions

ABSTRACT

This review is devoted to new rare earth–Mg–Ni-based (R–Mg–Ni-based) hydrogen storage alloys that have been developed over the last decade as the most promising next generation negative electrode materials for high energy and high power Ni/MH batteries. Preparation techniques, structural characteristics, gas–solid reactions and electrochemical performances of this system alloy are systematically summarized and discussed. The improvement in electrochemical properties and their degradation mechanisms are covered in detail. Optimized alloy compositions with high discharge capacities, good electrochemical kinetics and reasonable cycle lives are described as well. For their practical applications in Ni/MH batteries, however, it is essential to develop an industrial-scale homogeneous preparation technique, and a low-cost R–Mg–Ni-based electrode alloy (low-Co or Co-free) with high discharge capacity, long cycle life and good kinetics.

Contents

1. Introduction

Electrochemical energy storage and conversion systems have received an increasing amount of attention because of the rapid development of portable electronic devices and the requirement for a greener and less energy-intensive transportation industry [1–5]. A battery is a transducer that converts chemical energy into electrical energy, which contains mainly an electro-positive electrode (the anode), an electro-negative electrode (the cathode), a separator and an electrolyte [3]. Primary (non-rechargeable) and secondary (rechargeable) batteries exist [6,7] and secondary batteries can be restored to full charge by the application of electrical energy. This generally offers lower usage cost and longer service life than primary batteries [7]. Moreover, the proper selection of a secondary battery system reduces the amount of disposed toxic materials compared to an equivalent series of primary batteries.

Commonly used secondary batteries include lead-acid batteries, nickel–cadmium (Ni/Cd) batteries, nickel metal hydride (Ni/MH)

* Corresponding author. Tel.: +86 571 8795 2615; fax: +86 571 8795 2615.
E-mail address: hgpan@zju.edu.cn (H. Pan).

0925-8388/$ – see front matter © 2010 Elsevier B.V. All rights reserved.
doi:10.1016/j.jallcom.2010.08.157

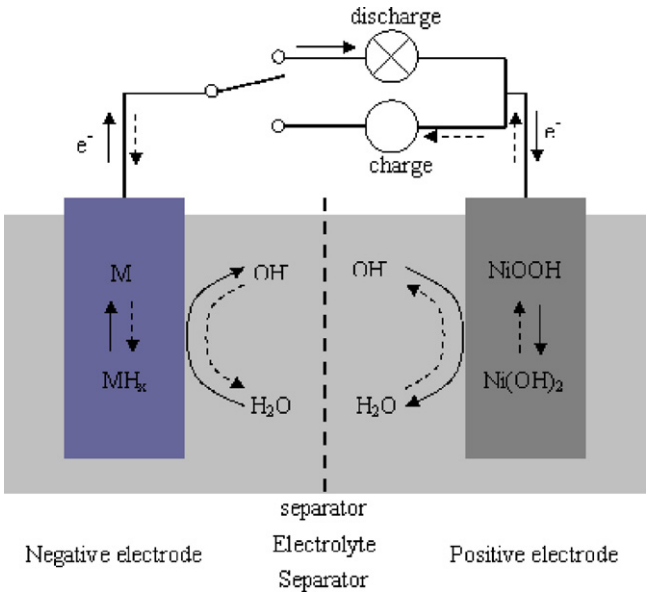

Fig. 1. Schematic diagram of the electrochemical charge–discharge reaction process of a Ni/MH battery.

batteries, lithium ion (Li-ion) batteries and lithium ion polymer (Li-ion polymer) batteries [5,7]. The Ni/MH battery was discovered in the 1970s [8,9] and introduced into market in the 1990s [10]. It is a new type of green rechargeable battery with a nickel hydroxide electrode as its positive electrode, a hydrogen storage alloy electrode as its negative electrode and a potassium hydroxide (KOH) solution as its electrolyte [6]. Fig. 1 shows schematically the electrochemical charge–discharge process of a Ni/MH battery. The overall electrochemical reaction of a Ni/MH battery can be described as follows [6,7,13]:

$$x\mathrm{Ni(OH)_2} + \mathrm{M} \underset{\text{discharge}}{\overset{\text{charge}}{\rightleftharpoons}} x\mathrm{NiOOH} + \mathrm{MH}_x \quad (1)$$

Upon charging, hydrogen atoms dissociate from $Ni(OH)_2$ at the positive electrode and are absorbed by the hydrogen storage alloy to form a metal hydride at the negative electrode. Upon discharging, the hydrogen atoms stored in the metal hydride dissociate at the negative electrode and react with NiOOH to form $Ni(OH)_2$ at the positive electrode. Therefore, the charge–discharge mechanism for a Ni/MH battery is merely a movement of hydrogen between a metal hydride electrode and a nickel hydroxide electrode in an alkaline electrolyte, *viz.*, the "rocking-chair" mechanism.

The Ni/MH battery has been widely used and quickly replaced the Ni/Cd battery for portable electronic applications because of its high energy density, long cycle life, high rate capacity, superior tolerance to overcharge/overdischarge and good environmental compatibility [2,6,7,11–13]. Today, it is the power source of choice for electric vehicles (EV) and hybrid electric vehicles (HEV), and is beginning to challenge the Ni/Cd battery for power tool applications [14]. The capacity, durability (cycle life) and dischargeability (kinetics) of Ni/MH batteries depend strongly on the intrinsic properties of the electrode materials, especially for hydrogen storage alloys used as negative electrode materials [4,6,7,13,15,16]. Hydrogen storage alloys are well known as a group of new functional intermetallics, which can reversibly absorb/desorb a large amount of hydrogen at or around standard temperatures and pressures [6,13,16]. A large number of hydrogen storage alloys have been developed as negative electrode materials for Ni/MH batteries, and these include AB_5-type rare earth-based alloys [6,13,14,15–21], AB_3- or A_2B_7-type rare earth–magnesium-based alloys [22–31], AB_2-type multicomponent alloys [31–36], Mg-based amorphous alloys [37–42] and Ti–V-based multiphase alloys [43–50]. Their performances differ greatly in terms of specific capacity, activation, rate dischargeability, and cyclic lifetime. AB_5-type rare earth-based alloys have been successfully used in Ni/MH batteries. However, it is increasingly difficult to meet the urgent demand for high-performance Ni/MH batteries from the rapid development of portable electronic devices because of their limited discharge capacity (~320 mAh/g). Recently, a new alloy family of AB_3- or A_2B_7-type rare earth–magnesium-based alloys with high specific capacity and good rate dischargeability was developed as the most promising next generation negative electrode materials for high energy and high power Ni/MH batteries. Numerous investigations have been conducted for their practical applications [22–30,51–109,111–122,124–130], especially in China and Japan. However, no systematical survey has been carried out on this newly developed hydrogen storage electrode alloy. This review essentially focuses on rare earth–Mg–Ni-based (R–Mg–Ni-based) hydrogen storage alloys with high energy densities and that are used as negative electrode materials in Ni/MH batteries. The preparation techniques, alloy compositions, structural features, gas–solid reaction and electrochemical properties of this system alloy are thoroughly described. Approaches for the improvement of their overall electrochemical performances are discussed as well.

2. Preparation and structural characteristics of R–Mg–Ni-based alloys

The electrode performances of Ni/MH batteries correlate closely to the compositions and microstructures of the hydrogen storage alloys [7], especially the composition homogeneity and the phase homogeneity of the alloys. Therefore, it is essential to develop suitable preparation techniques for homogeneous alloys with optimum and reproducible properties. In R–Mg–Ni-based alloys, the melting point of metallic Mg (650 °C) is obviously lower than that of the other constituent elements such as Ni (1455 °C), Co (1495 °C) and Mn (1244 °C), etc. [110]. The reduction of Mg volatilization to ensure a stable and homogeneous composition is of interest. Several preparation techniques such as powder sintering [22–27,30,51–56], vacuum magnetic levitation induction melting [28,29,57–92], arc melting [93–97], rapid solidification [89,98–103], spark plasma sintering [104], laser sintering [105] and ball milling [106–109] have been used to produce R–Mg–Ni-based hydrogen storage electrode alloys. Structures of the corresponding alloys have been characterized and identified by X-ray diffraction (XRD), scanning electron microscopy (SEM) and transmission electron microscope (TEM).

In 1980, Oesterreicher and Bittner [57] were the first to prepare single-phase ternary compounds with a C15-type structure ($La_{1-x}Mg_xNi_2$ (x = 0–0.67)) by induction melting on water-cooled copper boats under argon. Although Mg-rich $La_{1-x}Mg_xNi_2$ specimens appear to evolve hydrogen at room temperature, they did not attract attention for a long time because of their rather low hydrogen desorption rate caused by the highly stable hydride. Kadir et al. [22,24] successfully synthesized a series of new ternary R–Mg–Ni-based alloys, RMg_2Ni_9 (where R = La, Ce, Pr, Nd, Sm, Gd and Y) by sintering a mixture of $MgNi_2$ with RNi_5 intermetallic compounds or by directly sintering elements in an atomic ratio R:Mg:Ni = 1:2:9 as shown below:

$$\mathrm{RNi_5} + 2\mathrm{MgNi_2} \xrightarrow[6\text{ bar Ar}]{900-1100\,^\circ\mathrm{C}} \mathrm{RMg_2Ni_9} \quad (2)$$

$$\mathrm{R} + 2\mathrm{Mg} + 9\mathrm{Ni} \xrightarrow[6\text{ bar Ar}]{900-1100\,^\circ\mathrm{C}} \mathrm{RMg_2Ni_9} \quad (3)$$

These compounds crystallize in an ordered variant of the $PuNi_3$ type rhombohedral structure ($R\bar{3}m$ space group) which can be described as a stacking of RNi_5 and $MgCu_2$ ($MgZn_2$) units along

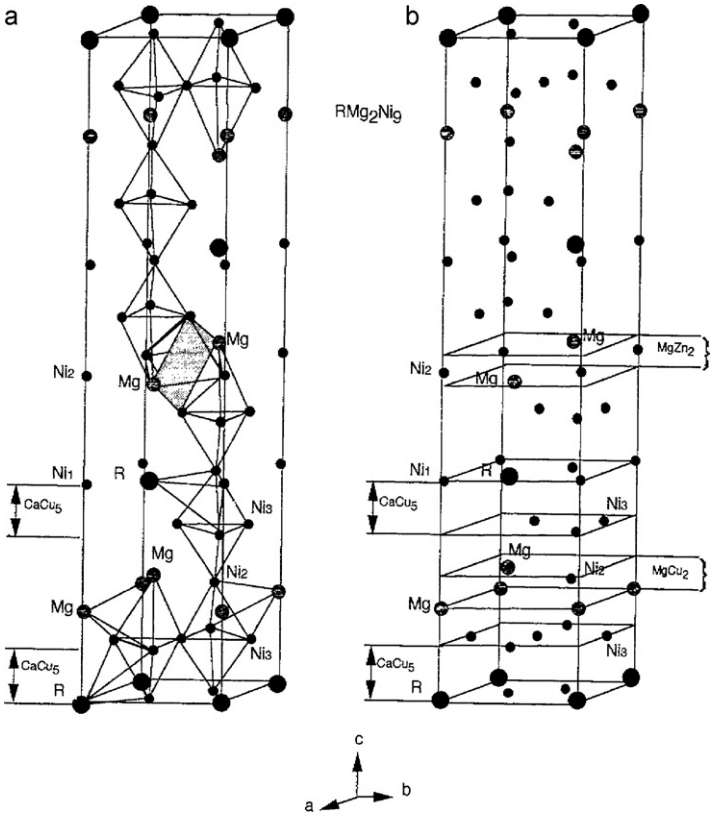

Fig. 2. Structural model of the RMg_2Ni_9 system alloys (where R = La, Ce, Pr, Nd, Sm, Gd and Y). (a) Arrangement of some of the tetrahedral of Ni atoms with Mg and R; (b) interrelation of stacking layers [22].

the *c*-axis as shown in Fig. 2. The R atoms occupy site 3*a* and the Mg atoms are located at site 6*c*. All the atoms at site 3*a* belong to the RNi_5 blocks whereas the atoms at position 6*c* are located in the $MgNi_2$ units. Three sites are available for Ni atoms: 3*b*, 6*c* and 18*h*. Table 1 lists the crystallographic parameters of YMg_2Ni_9 as an example [24].

The reports by Kadir et al. motivated intense interests in R–Mg–Ni-based hydrogen storage alloys. By a similar sintering process, Chen et al. [26,27] obtained several kinds of R–Mg–Ni-based alloys with a $PuNi_3$-type structure and these included $LaCaMgNi_9$, $LaCaMgNi_6Al_3$ and $LaCaMgNi_6Mn_3$, etc. Crystallographic results indicated that the Mg atoms only occupy 6*c* sites while the La and Ca atoms are located at the 3*a* and 6*c* sites. Almost simultaneously, Kohno et al. [28] prepared quaternary $La_{0.67}Mg_{0.33}Ni_{2.5}Co_{0.5}$, $La_{0.7}Mg_{0.3}Ni_{2.8}Co_{0.5}$ and $La_{0.75}Mg_{0.25}Ni_{3.0}Co_{0.5}$ alloys by induction melting under Ar gas at atmospheric pressure. However, they did not provide the detailed structural information for these alloys.

Following the aforementioned work, much research has been carried out on R–Mg–Ni-based hydrogen storage electrode alloys since 2003. Pan and co-workers [29,58–78] obtained a series of R–Mg–Ni-based alloys with a multiphase structure by vacuum magnetic levitation melting. Their compositions range from quaternary La–Mg–Ni–Co alloys to multinary La–Pr(Nd)–Mg–Ni–Co–Mn–Al alloys, which are mainly composed of a $LaNi_5$ phase and a $LaNi_3$ phase. Rietveld refinement reveals that Mg atoms exist only in the $LaNi_3$ phase and are located at the 6*c* sites [29]. Consequently, the $LaNi_3$ phase is expressed as a $(La,Mg)Ni_3$ phase or a $La(La,Mg)Ni_3$ phase in these cases. Liao et al. [30,51–55] synthesized La–Mg–Ni-based alloys with a stoichiometry of La_2MgNi_9 by a powder sintering method followed by annealing treatment. All sintered samples contained a $PuNi_3$-type primary phase and a few impurity phases like $LaNi_5$, $MgNi_2$ and La_2Ni_7, etc. At the same time, a number of La–Mg–Ni-based alloys with refined crystal grains were prepared by the rapid quenching technique [98–104]. XRD reveled that all quenched alloys possess a multiphase structure and TEM images showed that part of samples tended toward amorphization. Also, R–Mg–Ni-based alloys can be prepared by arc melting constituent elements on a water-cooled copper hearth under an argon atmosphere [100–104].

Recently, several new synthesis techniques have been used to prepare R–Mg–Ni-based hydrogen storage electrode alloys. Zhu et al. [106] obtained a nanocrystalline $Ml_{0.7}Mg_{0.3}Ni_{3.2}$ alloy by high energy ball milling and annealing. With increase milling time, the grain size decreased gradually and the AB_3 phase tended to transform into an AB_5 phase. After annealing treatment, the alloy was recrystallized and a decrease in the AB_3 phase with a corresponding increase in the AB_5 phase resulted. $La_{0.7}Mg_{0.3}Ni_{3.5}$–$Ti_{0.17}Zr_{0.08}V_{0.35}Cr_{0.1}Ni_{0.3}$ composites were obtained by ball milling the corresponding alloy powders under an argon atmosphere [109]. Results show that short-time ball milling does not change the structural features after a decrease in the average particle size. The $La_{0.7}Mg_{0.3}Ni_{3.5}$ alloy produced by green compact laser sintering $LaNi_5$, $MgNi_2$ and Ni mixtures is composed of Ce_2Ni_7, $LaNi_5$ and $LaMgNi_4$ phases [105]. With $LaNi_3$, Mg and carbonyl Ni powders as starting materials, Dong et al. [104] prepared $La_{0.80}Mg_{0.20}Ni_{3.75}$ alloy using spark plasma sintering. The product possesses a multiphase structure consisting of $(La,Mg)_2Ni_7$, $LaNi_5$ and Ni phases and their relative amounts correlate closely to the sintering temperatures.

To evaluate the quality of preparation techniques, Akiba et al. [111] analyzed the chemical compositions of quaternary La–Mg–Ni–Co alloys prepared by induction melting with inductively coupled plasma (ICP) spectrometry and energy-dispersive X-ray spectroscopy (EDX). Results show that their chemical composition is very close to the nominal composition. A similar phenomenon was also observed by Cuscueta et al. [84] with electron dispersion spectroscopy (EDS). Li et al. [112] determined that the loss of Mg in La–Mg–Ni-based alloys was more severe at higher annealing temperatures while the composition of the as-cast alloys was very close to the designed value. Moreover, an investigation into arc-melting alloys using ICP showed that the final composition was identical to the designed composition by the addition of a slight excess of Mg to compensate for the volatilization loss of Mg caused by its high vapor pressure [96]. It is therefore believed that the above-mentioned preparation techniques are reliable under optimized and controlled conditions.

Table 1
Crystallographic parameters for YMg_2Ni_9 in a space group $R\bar{3}m$ ($Z = 3$) [24].

Atoms	Site	Metal atom position			B_{iso} (Å^2)	Occupancy
		x	*y*	*z*		
Y	3a	0	0	0	1.51(1)	1
Mg	6c	0	0	0.1445(5)	0.86(2)	1
Ni1	3b	0	0	0.5	0.65(1)	1
Ni2	6c	0	0	0.3344(4)	0.75(2)	1
Ni3	18h	0.5019(6)	0.4981(6)	0.0848(2)	1.51(1)	1

3. Gas–solid reaction of R–Mg–Ni-based alloys

The electrochemical capacity of a hydride electrode is determined by its hydrogen absorption capability. In general, for electrochemical applications the most suitable hydrogen desorption plateau pressure of a metal hydride should be between 0.1 and 1 atm at room temperature [13]. Thus, to obtain the desired discharge capacity the nature of gas–solid reaction should be considered as represented by the pressure–composition–temperature

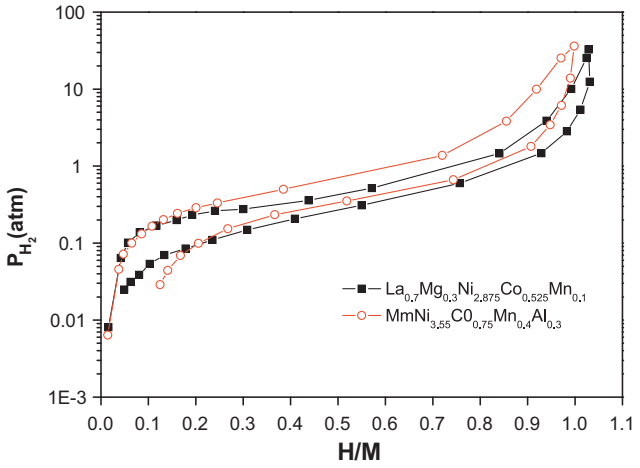

Fig. 3. Pressure–composition isotherms of the $AB_{3.5}$-type La–Mg–Ni-based alloy and the commercial AB_5-type alloy at 303 K [68].

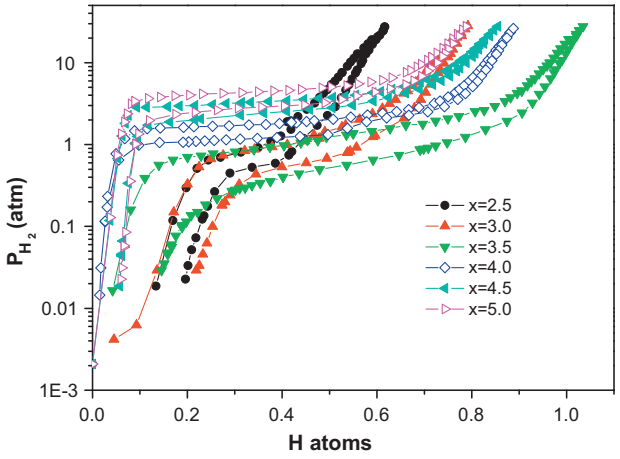

Fig. 4. Pressure–composition isotherms of the $La_{0.7}Mg_{0.3}(Ni_{0.85}Co_{0.15})_x$ (x = 2.5–5.0) hydrogen storage alloys at 303 K [29].

(PCT) curve, which consists of a family of isotherms that relate the hydrogen desorption equilibrium pressure to the amount of hydrogen stored in specimens. As described above, RMg_2Ni_9-type alloys can be regarded as ternary compounds built by a stacking of RNi_5 and $MgCu_2$ ($MgZn_2$) units. As a result, more hydrogen atoms are expected to be stored in RMg_2Ni_9-type alloys than in $LaNi_5$-type alloys.

Kadir et al. [22–25] pointed out that RMg_2Ni_9-type alloys have different hydriding/dehydriding behavior dependences on their constituent elements. It has been found that $LaMg_2Ni_9$ alloy stored only ~0.33 wt% (~0.2 H/M) with a plateau pressure of 2 atm at 303 K [25]. XRD analyses revealed that the $PuNi_3$-type structure remained unchanged after hydriding. Partial substitution of La and Mg with Ca increases the hydrogen storage capacity because of an increase in lattice parameters. It has also been found that ~1.87 wt% hydrogen is absorbed by the $(La_{0.65}Ca_{0.35})(Mg_{1.32}Ca_{0.68})Ni_9$ alloy and its unit cell volume increases by ~20% [25]. La_2MgNi_9-type alloys of $LaCaMgNi_9$, $La_{0.5}Ca_{1.5}MgNi_9$, $LaCaMgNi_6Al_3$ and $LaCaMgNi_6Mn_3$ are easily activated at room temperature under a hydrogen pressure of 3.3 MPa with a capacity of 0.9–1.1 H/M. PCT curves of $LaCaMgNi_9$, $LaCaMgNi_6Al_3$ and $LaCaMgNi_6Mn_3$ alloys show a single plateau region while $La_{0.5}Ca_{1.5}MgNi_9$ exhibits two plateaus [26]. Kohno et al. [28] reported that the hydrogen storage capability of the $La_{0.7}Mg_{0.3}Ni_{2.8}Co_{0.5}$ alloy is superior to that of the $MmNi_{4.0}Mn_{0.3}Al_{0.3}Co_{0.4}$ alloy. Moreover, the $AB_{3.5}$-type $La_{0.7}Mg_{0.3}Ni_{2.875}Co_{0.525}Mn_{0.1}$ alloy has better plateau performance and a larger hydrogen storage capacity than the AB_5-type $MmNi_{3.55}Co_{0.75}Mn_{0.4}Al_{0.3}$ alloy, as shown in Fig. 3 [68]. In the case of $La_{0.7}Mg_{0.3}(Ni_{0.85}Co_{0.15})_x$ (x = 2.5–5.0), the plateau region is larger and the plateau pressure remains almost unchanged when x increases from 2.5 to 3.5, whereas the width decreases and the plateau pressure rises gradually when x further increases to 5.0 (Fig. 4) [29]. The maximum hydrogen storage capacity of $La_{0.7}Mg_{0.3}(Ni_{0.85}Co_{0.15})_{3.5}$ alloy is about 1.03 H/M (~1.5 wt%) and the desorption plateau pressure is about 0.65 atm at 30 °C. Clearly, the hydrogen storage performance of R–Mg–Ni-based alloys correlates closely to their structural features especially their phase constitution and phase abundance [58–72].

Moreover, Peng and Zhu [113] showed that annealed $Ml_{0.7}Mg_{0.3}Ni_{3.2}$ alloy has a flatter pressure plateau and a larger hydrogen storage capacity than the as-cast alloy because of an increase in the abundance of the AB_3 phase after annealing. The maximum hydrogen storage capacity of $(LaPrNdZr)_{0.83}Mg_{0.17}(NiCoAlMn)_{3.3}$ alloy increases initially and then decreases with an increase in the annealing temperature [112], and the optimum storage capacity was obtained after annealing at 1198 K for 5 h. Energetic ball milling worsens hydrogen storage properties of $Ml_{0.7}Mg_{0.3}Ni_{3.2}$ alloy because of the formation of an amorphous phase [106]. Fortunately, a subsequent annealing treatment enables this alloy to gradually recover its hydrogen storage performance.

The influence of metallic elements like Co, Mn, Al, Ni, Mo, Mg, Ce and Nd on the hydrogen storage performance of AB_3- and $AB_{3.5}$-type La–Mg–Ni-based alloys has been widely investigated and discussed [30,51–55,58–72,83,85,94,97,114]. Liao et al. [30] examined the electrochemical PCT curves of $La_xMg_{3-x}Ni_9$ (x = 1.0–2.0) alloys at 25 °C. By decreasing Mg content, the plateau pressure for hydrogen absorption and desorption lowers noticeably and the plateau region becomes much wider and flatter, which leads to an increase in hydrogen storage capacity from 0.17 to 1.05 H/M. The increase in Mg content in $Ml_{1-x}Mg_xNi_{2.4}Co_{0.6}$ (x = 0–0.6) alloys decreases the stability of their hydrides [83]. An investigation into $La_{2-x}Mg_xNi_7$ (x = 0.3–0.6) alloys found similar behavior [114]. Partial substitution of Ce for La increases the plateau pressure for hydrogen absorption/desorption of $AB_{3.5}$- and $AB_{3.3}$-type La–Mg–Ni-based alloys associated with a decrease in hydrogen storage capacity because of cell volume shrinkage and changes in the phase content [63,94]. Appropriate substitution of La by Nd improves the hydrogen storage properties of $AB_{3.4}$-type La–Mg–Ni-based alloys [85]. The presence of Mn on the B side of $AB_{3.0-5.0}$-type La–Mg–Ni–Co-based alloys decreases the plateau pressure and increases the available hydrogen storage capacity for electrochemical applications [59–63]. Metallic Co plays a similar role to Mn in $AB_{3.5}$-type La–Mg–Ni–Co–Mn alloys [64]. An increase in Co content improves the hysteresis performance of hydrogen absorption/desorption and increases the plateau slope [64]. Higher Al substitution for Ni results in more stable hydrides and decreases the hydrogen storage capacity [67]. A similar phenomenon is observed for $La_{0.7}Mg_{0.3}Ni_{4.0-x}(Al_{0.5}Mo_{0.5})_x$ alloys as the desorption pressure continually reduces with an increase in Al and Mo. Obviously, the gas–solid reaction behavior of R–Mg–Ni-based hydrogen storage alloys can be tuned by modifying the composition and the type of annealing treatment. Therefore, the selection of a suitable alloy composition and proper preparation technique is required for optimum hydrogen storage performance.

4. Electrochemical properties of R–Mg–Ni-based alloys

The electrochemical properties of R–Mg–Ni-based alloys, including discharge capacity, activation, cycle stability, high rate dischargeability and electrochemical kinetic parameters, which are

Table 2
Properties of individual elements for R–Mg–Ni-based alloys.

Element	Selected properties	Ref.
La	Increase the unit cell volume Improve the plateau properties Increase the discharge capacity, easy activation and good high-rate dischargeability Poor cyclic stability due to the corrosion of La and large unit cell expansion rate	[30,51]
Mg	Eliminate the amorphization of hydrides Decrease the unit cell volume and the stability of hydride Increase the discharge capacity, the high-rate dischargeability and the cyclic stability	[57,70,83,84,114]
Ce	Decrease the unit cell volume Increase the plateau pressure of hydrogen absorption and desorption Reduce the hydrogen storage capacity Decrease the discharge capacity Improve the cyclic stability and increase the high-rate dischargeability	[66,94]
Pr and Nd	Decrease the lattice parameters and cell volumes of constitute phases Increase the plateau pressure of hydrogen desorption Decrease the maximum discharge capacity Improve the cyclic stability and the high-rate dischargeability	[76,78,85]
Zr	Decrease the cell volumes Decrease the maximum discharge capacity Improve the high-rate dischargeability	[74]
Co	Increase the lattice parameters and cell volumes Decrease the plateau pressure and the hysteresis of hydrogen absorption and desorption Increase the hydrogen storage capacity Improve effectively the cyclic stability due to the decrease of cell volume change and the increase of the suface passivation Increase the electrochemical kinetics	[53,64,65,88,92,116,117]
Mn	Increase the lattice parameters and cell volumes Facilitate the formation of $LaNi_5$ phase Decrease the plateau pressure Increase the maximum discharge capacity, improve the cyclic stability and increase the electrochemical kinetics	[52,59–63,86,96]
Al	Increase the lattice parameters and cell volumes Decrease the plateau pressure, increase the plateau slope and reduce the hydrogen storage capacity Improve significantly the cyclic stability due to the formation of a dense oxide film Decrease the maximum discharge capacity and the high-rate dischargeability	[54,67,72,87,90,91,95,118]
Fe and Cu	Decrease the discharge capacity, the high-rate dischargeability and the discharge potential Improve the cyclic stability	[101,102]
Cr	Increase the unit cell volumes Decrease the discharge capacity Improve the cyclic stability Decrease the high-rate dischargeability	[77,99]
W and Mo	Decrease the maximum discharge capacity Increase the cyclic stability and the high-rate dischargeability due to the presence of the desirable surface properties and the increase of electronic or ionic conductivities	[75,90,95]

dependent on alloy composition and structural features, have been extensively investigated over the last decade and the degradation mechanisms of R–Mg–Ni-based alloy electrodes have been elucidated as well [27–30,51–122,124–130]. Table 2 summarizes detailed information about the function of the individual elements used in R–Mg–Ni-based alloys. Optimized R–Mg–Ni-based electrode alloys have been produced for high-energy and high-power Ni/MH batteries, as shown in Table 3.

4.1. Composition modifications

As the active material of the negative electrodes in Ni/MH batteries, hydrogen storage alloys play several important roles including that of an electrochemical catalyst for hydrogen generation/oxidation and a hydrogen storage reservoir/hydrogen source during charge/discharge. Thus, a reasonable compositional change is required for high discharge capacity, good electrochemical activity and corrosion resistance. A large amount of work has been carried out on this subject and the effects of stoichiometry and substitution elements have been investigated and reported [27–30,51–114].

4.1.1. Stoichiometry optimization

In 2000, Kohno et al. [28] studied (La,Mg)$(NiCo)_x$ (x = 3.0–3.5) system alloys with compositions $La_{0.67}Mg_{0.33}Ni_{2.5}C0_{0.5}$, $La_{0.7}Mg_{0.3}Ni_{2.8}C0_{0.5}$ and $La_{0.75}Mg_{0.25}Ni_{3.0}Co_{0.5}$. Among them, the $La_{0.7}Mg_{0.3}Ni_{2.8}Co_{0.5}$ alloy had a discharge capacity as large as 410 mAh/g, which is 1.3 times larger than that of AB_5-type alloys. This discovery led to a great deal of interest in La–Mg–Ni-based alloys as high-energy density negative electrode materials. Pan et al. [29] formulated a series of $La_{0.7}Mg_{0.3}(Ni_{0.85}Co_{0.15})_x$ (x = 2.5–5.0) alloys and found that all the important electrochemical properties of these alloy electrodes including maximum discharge capacity, high rate dischargeability, exchange current density and limiting current density increased as x increased from 2.5 to 3.5 and then decreased with a further increase in x because of the change in alloy composition and phase structure. The maximum discharge capacity of $La_{0.7}Mg_{0.3}(Ni_{0.85}Co_{0.15})_{3.5}$ alloy is about 396 mAh/g, which is far higher than conventional AB_5-type alloys and it provides a starting alloy composition for the further improvement of the electrochemical performance of La–Mg–Ni–Co-based alloys [58–78]. Unfortunately, this system alloy exhibits poor cycling durability in alkaline electrolytes (Fig. 5) [29]. After 60 cycles, the capacity retention ($C_{60}/C_{max} \times 100\%$) of $La_{0.7}Mg_{0.3}(Ni_{0.85}Co_{0.15})_{3.5}$ alloy is only 45.9% when measured using a charge current density of 100 mAh/g and a discharge current density of 60 mA/g. A recent electrochemical examination on annealed $La_{0.7}Mg_{0.3}(Ni_{0.9}Co_{0.1})_x$ (x = 3.0–3.8) alloys found an increase in the maximum discharge capacity from 356.6 mAh/g (x = 3.0) to 392.1 mAh/g (x = 3.5) and then a decrease to 344.1 mAh/g (x = 3.8) [81]. These results are

Table 3
Structures and electrochemical properties of various R–Mg–Ni-based alloy electrodes.

Alloy	Preparation method[a]	Structure	Electrochemical properties						Ref.
			Measurement system	Charge/discharge current density (mAh/g)	Compacting materials (Powder)	Maximum discharge capacity (mAh/g)	High-rate dischargeability	Capacity retention	
La_2MgNi_9	S	$PuNi_3$-type	Tri-electrode	300/100	Ni	397.5	HRD_{1200} = 52.7%	S_{100} = 60.6%	[51]
$Ml_{0.7}Mg_{0.3}Ni_{3.2}$	IM + BM	Amorphous phase	Tri-electrode	100/50	Ni	105	–	S_{20} = 62%	[114]
$La_{0.8}Mg_{0.2}Ni_{3.75}$	SPS(1223K)	$(La,Mg)_2Ni_7$ $LaNi_5$	Tri-electrode	60/60	Ni	368.2	HRD_{900} = 60.75%	S_{150} = 58.4%[b]	[105]
$La_{0.7}Mg_{0.3}Ni_{3.5}$	LS(1200W)	Ce_2Ni_7-type $LaNi_5$ $LaMgNi_4$	Tri-electrode	100/50	Cu	352.8	HRD_{800} = 79.4%	S_{100} = 58.4%	[106]
$La_{0.75}Mg_{0.25}Ni_{3.5}$	IM	$(La,Mg)_2Ni_7$ $LaNi_5$	Tri-electrode	60/60	Ni	343.7	HRD_{900} = 77.96%	S_{100} = 55.83%	[82]
$La_{1.5}Mg_{0.5}Ni_7$	IM + A	$(La,Mg)_2Ni_7$ $LaNi_5$	Tri-electrode	100/100	Ni	389.48	HRD_{900} = 92.3%	S_{70} = 85.8%	[115]
$LaCaMgNi_9$	S	$PuNi_3$-type	Two-electrode	150/150	Ni	356	–	–	[27]
$La_{0.7}Mg_{0.3}Ni_{2.8}Co_{0.5}$	IM	–	Tri-electrode	100/100	Cu	410	–	–	[28]
$La_{0.7}Mg_{0.3}(Ni_{0.85}Co_{0.15})_{3.5}$	VMLM	$(La,Mg)Ni_3$ $LaNi_5$	Tri-electrode	100/60	Ni	395.6	HRD_{1000} = 85.8%	S_{60} = 45.9%	[29]
$La_2Mg(Ni_{0.8}Co_{0.2})_9$	S	$PuNi_3$-type	Tri-electrode	200/50	Ni	404.5	HRD_{800} = 64.2%	S_{100} = 69.3%	[53]
$La_2Mg(Ni_{0.98}Co_{0.02})_9$	S	$PuNi_3$-type La_2Ni_7	Tri-electrode	200/50	Ni	374.5	HRD_{800} = 13.8%	S_{150} = 73.8%	[54]
$La_{0.7}Mg_{0.3}(Ni_{0.9}Co_{0.1})_{3.5}$	IM + A	$(La,Mg)Ni_3$ $(La,Mg)_2Ni_7$	Two-electrode	60/60	Ni	392.1	–	S_{100} = 93.5%[c]	[81]
$Ml_{0.6}Mg_{0.4}Ni_{2.4}Co_{0.6}$	IM + A	$LaNi_3$ $LaNi_5$ $LaNi_2$	Tri-electrode	100/100	–	326	HRD_{1200} = 40%	S_{100} = 80%	[83]
$La_{1.5}Mg_{0.5}Ni_{5.2}Co_{1.8}$	IM + A	$PuNi_3$ Ce_2Ni_7	Tri-electrode	100/100	Ni	405.69	HRD_{900} = 90.64%	S_{70} = 68.9%	[88]
$La_{0.7}Mg_{0.3}Ni_{2.65}Mn_{0.1}Co_{0.75}$	VMLM	$(La,Mg)Ni_3$ $LaNi_5$	Tri-electrode	100/60	Ni	403.1	HRD_{1500} = 69.2%	S_{90} = 36.9%	[65]
$La_{0.7}Mg_{0.3}Ni_{2.9}(Al_{0.5}Mo_{0.5})_{0.6}$	AM	$La(La,Mg)_2Ni_9$ $LaNi_5$ $LaNi$	Tri-electrode	60/60	Ni	397.6	HRD_{1200} = 70.5%	S_{70} = 70.8%	[95]
$Ml_{0.8}Mg_{0.2}Ni_{3.2}Co_{0.4}Al_{0.2}$	IM	$LaNi_5$ $LaNi_3$	Tri-electrode	100/100	–	327	HRD_{1200} = 59%	S_{300} = 89%[b]	[87]
$La_{0.7}Mg_{0.3}Ni_{3.4}(MnAl_2)_{0.1}$	VMLM	$(La,Mg)Ni_3$ $LaNi_5$	Tri-electrode	300/100	Ni	355.2	HRD_{800} = 79%	S_{100} = 43.7%	[91]
$La_{0.7}Mg_{0.3}Ni_{2.45}Mn_{0.1}Co_{0.75}Al_{0.2}$	VMLM	$(La,Mg)Ni_3$ $LaNi_5$	Tri-electrode	100/60	Ni	370	HRD_{1000} = 71.3%	S_{100} = 67.1%	[67]
$La_{0.4}Nd_{0.4}Mg_{0.2}Ni_{3.2}Co_{0.2}Al_{0.2}$	IM + A	$LaNi_5$ La_2Ni_7 $LaNi_3$	Tri-electrode	60/60	Ni	372	HRD_{1200} = 39.2% (C_d/C_{60})	S_{100} = 82.3%	[85]

$La_{1.3}CaMg_{0.7}Ni_{8.7}(Al_{0.5}W_{0.5})_{0.3}$	IM	(La,Mg)Ni_3 $LaNi_5$ $(La,Mg)_2Ni_7$	Tri-electrode	100/100	–	365.6	HRD_{900} = 63.2%	S_{100} = 73.27%[b]	[90]
$La_{0.55}Pr_{0.15}Mg_{0.3}Ni_{2.45}Co_{0.75}Mn_{0.1}$	VMLM	(La,Mg)Ni_3 $LaNi_5$	Tri-electrode	100/60	Ni	356.8	HRD_{1000} = 78.9%	S_{80} = 79.4%	[76]
$La_{0.6}Pr_{0.1}Mg_{0.3}Ni_{2.45}Co_{0.75}Mn_{0.1}$	VMLM	(La,Mg)Ni_3 $LaNi_5$	Tri-electrode	100/60	Ni	372.7	HRD_{1000} = 70.1%	S_{100} = 78.4%	[78]
$La_{0.7}Mg_{0.3}Ni_{2.4}Cr_{0.05}Co_{0.75}Mn_{0.1}Al_{0.2}$	VMLM	(La,Mg)Ni_3 $LaNi_5$	Tri-electrode	100/60	Ni	358.5	HRD_{750} = 67.2%	S_{100} = 70%	[77]
$La_{0.5}Ce_{0.2}Mg_{0.3}Co_{0.4}Ni_{2.4}Mn_{0.2}$	Q	(La,Mg)Ni_3 $LaNi_5$	Tri-electrode	100/100	Ni	351.32	–	–	[104]
$La_{0.7}Mg_{0.3}Ni_{3.5}$– $40\%Ti_{0.17}Zr_{0.08}V_{0.35}Cr_{0.1}Ni_{0.3}$	BM	(La,Mg)Ni_3 $LaNi_5$ LaNi BCC	Tri-electrode	300/100	Ni	335.2	–	S_{70} = 63%	[110]
$(La_{0.205}Pr_{0.392}Nd_{0.392}Zr_{0.012})_{0.83}$– $Mg_{0.17}Ni_{2.97}Co_{0.1}Al_{0.2}Mn_{0.03}$	IM + A	C14 Laves Ce_2Ni_7-type $CaCu_5$-type Ce_5Co_{19}-type	Tri-electrode	100/70	Ni	345	–	S_{50} = 90.7%	[113]

[a] S, sintering; IM, induction melting; BM, ball milling; SPS, spark plasma sintering; LS, laser sintering; A, annealing; VMLM, vacuum magnetic levitation melting; AM, arc melting; Q, quenching.
[b] Charge/discharge current density: 600 mA/g.
[c] Charge/discharge current density: 300 mA/g.

Fig. 5. Discharge capacity vs. cycle number of the $La_{0.7}Mg_{0.3}(Ni_{0.85}Co_{0.15})_x$ (x = 2.5–5.0) hydrogen storage alloys at 303 K [29].

in good agreement with the report of Pan et al. [29]. Therefore, varying the stoichiometric ratio could be used to roughly optimize the alloy composition and phase structure of hydrogen storage electrode alloys.

4.1.2. A-side substitution

Liao et al. [30,51] prepared $La_xMg_{3-x}Ni_9$ (x = 1.0–2.2) alloys and found that La-rich alloys (x = 1.8–2.1) possessed promising electrode properties including a large discharge capacity (~ 400 mAh/g), easy activation and good high-rate dischargeability, although cyclic durability was needed for further improvement. A specific amount of Mg substitution for La in the $La_{2-x}Mg_xNi_{7.0}$ (x = 0.3–0.6) alloys increases its maximum discharge capacity and enhances its electrochemical kinetics [114]. However, its cyclic stability deteriorates with increasing Mg substitution because of more serious corrosion and pulverization. An increase in the La/Mg ratio in $La_{0.75+x}Mg_{0.25-x}Ni_{3.5}$ (x = 0–0.1) alloys improves the cycling stability of the alloy electrodes but decreases their discharge capacity and high-rate dischargeability [82]. The cycle life of the $Mm_{0.83}Mg_{0.17}Ni_{3.1}Al_{0.2}$ alloy is 2.5 times longer than that of the $Mm_{0.7}Mg_{0.3}Ni_{3.1}Al_{0.2}$ alloy, measured using 1500 mAh AA size batteries [115]. For $Ml_{1-x}Mg_xNi_{2.4}Co_{0.6}$ (x = 0–0.6) alloys, however, a higher Mg content leads to a larger discharge capacity, better high-rate dischargeability and longer cycling durability because of the reduction of unit cell volume and a decrease in decrepitation upon cycling [83].

To improve the cyclic durability and to cut the cost of R–Mg–Ni-based alloys, La has been partially substituted by Ce in the $La_{0.7-x}Ce_xMg_{0.3}Ni_{2.875}Co_{0.525}Mn_{0.1}$ (x = 0–0.5) alloys [66]. By increasing Ce content, the cycling stability of the alloy electrodes improved as expected because the capacity decay rate decreased from 2.65 mAh/g cycle (x = 0) to 0.10 mAh/g cycle (x = 0.5). Two major factors govern the effects of Ce on electrochemical cycling stability. First is that an increase in Ce content leads to a smaller change in the unit cell upon hydriding and hence less pulverization. Second is the formation of a protective surface film which effectively inhibits further oxidation of the alloy and slows down the corrosion rate. However, a big problem with increasing Ce content is that the discharge capacity is dramatically decreased from 382 mAh/g (x = 0) to 48.6 mAh/g (x = 0.5). Zhang et al. [94] observed a similar phenomenon for the $La_{0.7-x}Ce_xMg_{0.3}Ni_{2.8}Co_{0.5}$ alloys. Thus, the Ce content should be carefully considered before use in R–Mg–Ni-based electrode alloys.

Recently, Pan et al. [76,78] investigated the function of Pr and Nd in $La_{0.7-x}R_xMg_{0.3}Ni_{2.45}Co_{0.75}Mn_{0.1}Al_{0.2}$ (R = Pr and Nd, x = 0.0–0.3) alloys. They found that Pr and Nd have similar effects in La–Mg–Ni–Co–Mn–Al-type alloys. An increase in Pr and Nd content in the alloys decreases maximum discharge capacity, improves cycling stability and enhances electrochemical kinetics. Similar behavior was found for $La_{0.75-x}Pr_xMg_{0.25}Ni_{3.2}Co_{0.2}Al_{0.1}$ alloys [125]. The decrease in maximum discharge capacity is attributed to a reduction in the abundance of the (La,Mg)Ni_3 phase. This change in phase abundance and the reduction in unit cell volume lead to an improvement in the electrochemical kinetic properties. In addition, the higher anisotropy factor c/a, which results from the presence of Pr and Nd, is responsible for the improvement in cyclic stability. Considering the overall effects of partial substitution of La with Pr and Nd on $La_{0.7-x}R_xMg_{0.3}Ni_{2.45}Co_{0.75}Mn_{0.1}Al_{0.2}$ alloy electrodes, the optimized compositions were found to be x = 0.15 for Pr and x = 0.1 for Nd [76,78]. The introduction of Zr into $La_{0.7-x}Zr_xMg_{0.3}Ni_{2.45}Co_{0.75}Mn_{0.1}Al_{0.2}$ (x = 0–0.1) alloys decreases discharge capacity, but improves high-rate dischargeability [74]. The optimum substitution of Zr for La is x = 0.02 for the enhancement of electrochemical kinetics. However, the electrochemical cycling stability remains almost unchanged over the measured composition range. A small amount of Ti for La substitution in AB_3-type $(La_{1-x}Ti_x)_{0.67}Mg_{0.33}Ni_{2.75}Co_{0.25}$ hydrogen storage alloys is also effective in improving the overall electrochemical properties [126].

4.1.3. B-side substitution

For a hydrogen storage electrode alloy, the B-side component generally consists of metallic elements with a weak hydrogen affinity (transition metals from Groups 5–10), which determines its catalytic activity and chemical stability [4]. The optimization of the B-side component can improve the discharge capacity, activation, high-rate dischargeability and/or cyclic stability (Table 2). Consequently, it is regarded as one of the most effective ways to improve the electrochemical performance of hydrogen storage electrode alloys.

Co, Cu and Mn substituted $La_2Mg(Ni_{0.95}M_{0.05})_9$ quaternary alloys show a slight reduction in discharge capacity and moderate improvement in cycle stability [52]. The influence of Ni replacement by Mn on the electrochemical properties of $AB_{3.0-5.0}$-type La–Mg–Ni–Co alloys was studied systematically by Pan and co-workers [59–63]. All the alloys exhibited good electrochemical activation. For $AB_{3.0}$-, $AB_{4.0}$-, $AB_{4.5}$- and $AB_{5.0}$-type alloys, appropriate substitution of Ni with Mn increases the discharge capacity of the alloy electrodes because of the optimized phase structure and the decreased desorption plateau pressure. However, the maximum discharge capacity of the $AB_{3.5}$-type alloy is first almost unchanged and then decreases with an increase in Mn content. The electrochemical kinetic properties of all the alloy electrodes improve after partial substitution of Ni by Mn because the dissolution of Mn into the electrolyte leads to an increase in Ni content on the alloy surface upon cycling. However, their cyclic stabilities do not change noticeably. Recent investigations on Mn-substituted $AB_{3.5}$-type $ReNi_{2.6-x}Mn_xCo_{0.9}$ alloys present similar results [127]. The low-temperature dischargeability of $La_{0.7}Mg_{0.3}Ni_{2.975-x}Co_{0.525}Mn_x$ (x = 0–0.4) alloy electrodes increases remarkably with an increase in Mn content because of the increase in hydrogen diffusion coefficient caused by cell volume expansion [96]. Moreover, specific amount of Mn incorporated into $La_{0.7}Mg_{0.3}Ni_2Co_{1-x}Mn_x$ alloys prolongs the cycle life of the alloy electrodes and decreases the maximum discharge capacity [86].

Metallic Co is a very important element for improving the overall electrochemical properties of rare earth based hydrogen storage electrode alloys, especially for prolonging their cycle lives [6,7,16]. The roles played by Co in La–Mg–Ni-based electrode alloys have been extensively studied and elaborated [53,65,88,92,116,117,128]. Liu et al. [65] revealed in detail the effects of Co content on the electrochemical properties of $La_{0.7}Mg_{0.3}Ni_{3.4-x}Mn_{0.1}Co_x$ (x = 0–1.6) alloy electrodes by a series of electrochemical measurements. Firstly, partial substitution of Ni with Co effectively improves the cyclic stability of La–Mg–Ni–Mn–Co system alloys with a slight loss of maximum discharge capacity (Fig. 6), which is due to a relatively smaller cell volume change during charging/discharging and an increase in surface passivation. Secondly, the appropriate substitution of Co for Ni increases the electrochemical kinetic performance of the alloy electrodes because of the concentration of Co and Ni on the surface of the alloy particles and the subsequent formation of a Raney Ni-Co film with relatively higher electrocatalytic activity. Taking into account the overall electrochemical performance and cost of the alloy, the optimum content of Co in $La_{0.7}Mg_{0.3}Ni_{3.4-x}Mn_{0.1}Co_x$ alloys for the negative electrodes in Ni/MH secondary batteries should be within x = 0.75–1.15 [65]. However, an increase in Co substitution decreases the high-rate dischargeability (HRD) of $La_2Mg(Ni_{1-x}Co_x)_9$ (x = 0.1–0.5) alloys [53]. Lower Co substitution ($x \leq 0.2$) results in a slight decrease in the HRD because of a decrease in electrocatalytic activity for the charge-transfer reaction. At a Co substitution of more than 0.2, the HRD decreases sharply because of the lower hydrogen diffusion rate in the alloy bulk. $La_{0.67}Mg_{0.33}Ni_{3.0-x}Co_x$ alloys and $La_{1.5}Mg_{0.5}Ni_{7-x}Co_x$ alloys have a large discharge capacity (>390 mAh/g) and good activation ability [88,116]. Strangely, their cyclic durability becomes worse with an increase in Co content, especially for the $La_{1.5}Mg_{0.5}Ni_{7-x}Co_x$ alloys, which differs from all the other reports. Optimized electrochemical kinetics was achieved for the alloy electrode with x = 0.3. However, the discharge capacities of $La_{0.75}Mg_{0.25}Ni_{3.5}Co_x$ and $La_{0.75}Mg_{0.25}Ni_{2.5}Co_x$ alloys increased dramatically after the addition of a specific amount of Co [92,117].

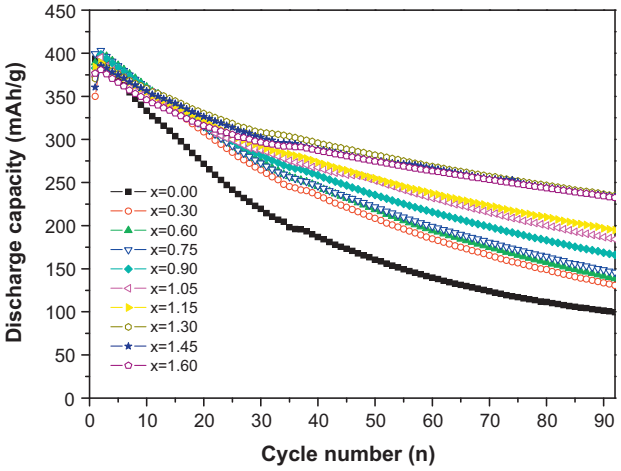

Fig. 6. Cyclic stability of the $La_{0.7}Mg_{0.3}Ni_{3.4-x}Mn_{0.1}Co_x$ (x = 0.0–1.6) alloy electrodes at 303 K [65].

Al in La–Mg–Ni-based alloys has been found to improve the cyclic durability of alloy electrodes [54,67,72,87,90,91,95,118]. Increasing Al content in AB_3-type $La_2Mg(Ni_{1-x}Al_x)_9$ (x = 0–0.05) alloys leads to a decrease in the discharge capacity and electrochemical kinetics but the cyclic stability of the alloy electrodes improves significantly [54]. The cyclic durability of $La_{0.7}Mg_{0.3}Ni_{2.65-x}Mn_{0.1}Co_{0.75}Al_x$ (x = 0–0.05) alloy electrodes improves noticeably as the capacity retention after 100 cycles increases from 32.0% (x = 0) to 73.8% (x = 0.3) (Fig. 7) [67]. Investigations on $La_{0.7}Mg_{0.3}Ni_{2.55-x}Co_{0.45}Al_x$ alloys and $Ml_{0.8}Mg_{0.2}Ni_{3.2}Co_{0.6-x}Al_x$ alloys further confirm the improvement in cyclic stability [87,118]. This is explained by a decrease in

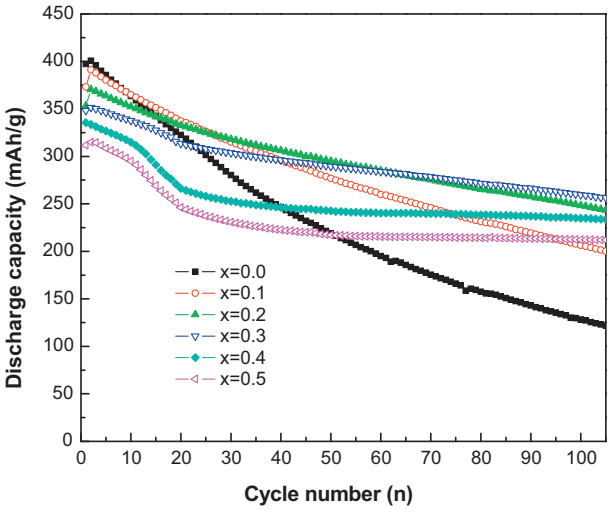

Fig. 7. Cyclic stability of the $La_{0.7}Mg_{0.3}Ni_{2.65-x}Mn_{0.1}Co_{0.75}Al_x$ (x = 0–0.5) alloy electrodes at 303 K [67].

the pulverization of the alloy particles during charge/discharge cycling because of smaller cell volume expansion and contraction, and an increase in anti-oxidation/corrosion because of the formation of a dense Al oxide film upon cycling. The latter is the most important reason for the improvement in cycling stability of La–Mg–Ni–Co–Mn–Al type alloy electrodes [72]. The electrochemical reaction kinetics of $La_{0.7}Mg_{0.3}Ni_{3.5-x}(MnAl_2)_x$ (x = 0–0.2) alloys decreases when $x < 0.1$ because of an increase in the charge-transfer resistance, which is caused by the formation of an Al-containing passive film [91]. When $x > 0.1$, the electrochemical kinetics increases because the Al oxide film on the electrode surface is cracked and this is caused by the dissolution of Mn into the alkaline electrolyte. The co-substitution of Al–W [90] and Al–Mo [95] for Ni noticeably improved the cyclic stability of AB_3-type $La_{1.3}CaMg_{0.7}Ni_{9-x}(Al_{0.5}W_{0.5})_x$ and $La_{0.7}Mg_{0.3}Ni_{3-x}(Al_{0.5}Mo_{0.5})_x$ alloys while their discharge capacities decreased. The high-rate dischargeabilities decreased initially and then increased with an increasing Al–W and Al–Mo content because of the interaction of Al and W (Mo). However, an increase in Al–Mo content in $AB_{3.5}$-type $La_{0.7}Mg_{0.3}Ni_{3.5-x}(Al_{0.5}Mo_{0.5})_x$ alloys results in a linear increase in the high-rate dischargeability [95].

The substitution of Ni by other transition metals like W, Fe, Cu and Cr in La–Mg–Ni–Co-based electrode alloys has also been studied [75,77,99,101,102,129]. Specific amounts of W (x = 0.02–0.05) in $AB_{3.5}$-type $La_{0.7}Mg_{0.3}Ni_{2.45-x}Co_{0.75}Mn_{0.1}Al_{0.2}W_x$ alloys imparts desirable surface properties and improves electronic or ionic conductivities of the alloys, consequently ameliorating the cyclic stability and electrochemical kinetics of the alloy electrodes [75]. The introduction of Fe and Cu into AB_3-type $La_{0.7}Mg_{0.3}Ni_{2.55-x}Co_{0.45}M_x$ (M = Fe or Cu) alloys improves the cyclic stability of the alloy electrodes because of an increase in their anti-pulverization abilities but it also reduces their maximum discharge capacity [101,102,129]. Miao et al. [77] reported that the formation of a dense Cr-oxide film on the alloy surface increased the cyclic stability of $La_{0.7}Mg_{0.3}Ni_{2.45-x}Cr_xCo_{0.75}Mn_{0.1}Al_{0.2}$ alloys with x = 0.05–0.10. Wang et al. [99] also found that the addition of Cr into $La_2Mg(Ni_{0.85}Co_{0.15})_9Cr_x$ alloys increased the cyclic durability of alloy electrodes because of an increase in their anti-corrosion ability.

4.2. Heat treatment

Annealing treatment is very useful to eliminate component segregation and to improve the structure of hydrogen storage alloys, consequently leading to an improvement in the overall electrochemical properties [13]. Pan et al. [119–121] first reported the effects of annealing treatment on La–Mg–$(NiCo)_x$ (x = 3.0–3.5) alloys and found that $La_{0.7}Mg_{0.3}Ni_{2.8}Co_{0.5}$ alloy annealed at 1123 K for 8 h exhibited a large discharge capacity of 414 mAh/g, a longe cycle life and better electrochemical kinetics because of the homogenization of the composition and structure. Further investigation showed that higher annealing temperature (1273–1373 K × 8 h) reduces the maximum discharge capacity because of a change in the phase abundance and deteriorates the high rate dischargeability due to an increase in its anti-pulverization property and a reduction in defects although the cyclic stability of $AB_{3.5}$-type $La_{0.7}Mg_{0.3}Ni_{2.45}Co_{0.75}Mn_{0.1}Al_{0.2}$ alloy improved significantly [73]. The maximum discharge capacity of the $Ml_{0.7}Mg_{0.3}Ni_{3.2}$ alloy that was ball-milled for 20 min increased more than 1.5 times after being annealed at 900 °C for 4 h because of recrystallization [113]. Moreover, the discharge capacity, cyclic stability and high rate dischargeability of $La_{0.8}Mg_{0.2}Ni_{2.4}Mn_{0.1}Co_{0.55}Al_{0.1}$ alloy improved obviously after annealing at 1173 K for 7 h [122]. The annealed $(LaPrNdZr)_{0.83}Mg_{0.17}(NiCoAlMn)_{3.3}$ alloy has an increased discharge capacity and improved electrochemical kinetics while its cycling capacity retention decreased because of the formation of a new phase with a $CeNi_3$-type structure, which was caused by the presence of Pr and Nd [112]. We believe that annealing treatment leads to different effects for La–Mg–Ni-based electrode alloys with different compositions.

Hydrogen storage electrode alloys with small crystal grains are usually prepared by rapid quenching and melt spinning [123]. Zhang et al. [89,98–104] prepared a series of La–Mg–Ni-based electrode alloys by rapid quenching and studied the effects of the solidification rate on their electrochemical properties. They found that the rapid quenching obviously enhances the cyclic stability of the alloy electrodes because of the reduction in grain size, but the discharge capacity and activation performance decreased.

4.3. Ball milling, surface treatment and electrolyte modification

Other methods such as ball milling treatment, surface treatment and electrolyte modification have been used to ameliorate the electrode performance of R–Mg–Ni-based alloys [106–109,113]. The $Ml_{0.7}Mg_{0.3}Ni_{3.2}$ alloy ball-milled for 20 min only discharges 105 mAh/g [113], which is obviously lower than its theoretical capacity of 455 mAh/g because of the formation of a nanocrystalline phase [106]. The discharge capacity of $La_{0.7}Mg_{0.3}Ni_{3.5}$–$Ti_{0.17}Zr_{0.08}V_{0.35}Cr_{0.1}Ni_{0.3}$ composite electrode decreases with an increase in ball milling time [109]. Surface treatment has also been employed to improve the electrochemical properties of $La_{0.7}Mg_{0.3}Ni_{2.4}Co_{0.6}$ alloy [93]. After surface treatment with KBH_4, KOH and KOH containing KBH_4, the discharge capacity, cyclic stability and electrochemical kinetics of the alloy electrodes increased markedly, especially for alloys treated by KOH containing KBH_4. The addition of $Cu(OH)_2$ to a 6 mol/L KOH electrolyte lowers the activation property and high rate dischargeability of $La_2Mg_{0.9}Al_{0.1}Ni_{7.5}Co_{1.5}$ alloy electrode. However, the cyclic stability improves dramatically due to the formation of a Cu film on the surface of the alloy electrode [124].

4.4. Temperature effect

The operating temperature has a noticeable effect on the capacity and voltage characteristics of Ni/MH batteries [131]. Liu et al. [68] systematically investigated the electrochemical performance of $La_{0.7}Mg_{0.3}Ni_{2.875}Co_{0.525}Mn_{0.1}$ alloy from −20 to 30 °C and found that the operating temperatures had a striking effect on the overall electrochemical properties, especially on the electrochemical kinetics. The discharge capacity and high-rate dischargeability of

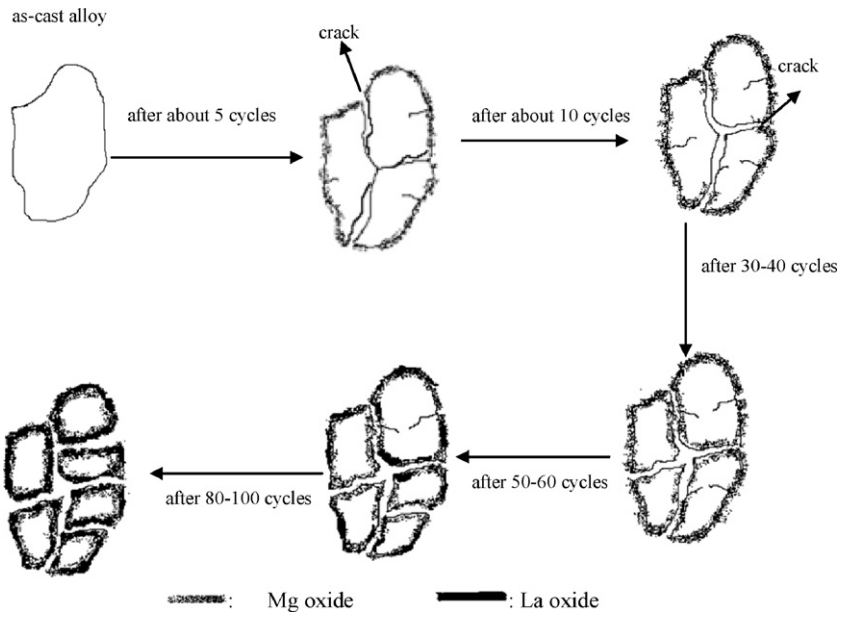

Fig. 8. Schematic model of disintegration and surface oxidation for La–Mg–Ni–Mn alloy powder during charge/discharge cycling [69].

the alloy electrode decreased with decreasing testing temperature due to slower hydrogen transfer in the bulk and lower electrocatalytic activity at low temperatures. In-depth studies on kinetic parameters indicate that the diffusion of hydrogen in the bulk is the rate-determining factor for the discharge process of La–Mg–Ni–Co-based alloy electrodes at temperatures above 10 °C while the charge-transfer reaction is rate-determining at lower temperatures (<10 °C). Zhang et al. [94–96] also reported that the substitution of Mn and Al–Mo for Ni enhanced the low-temperature dischargeability of La–Mg–Ni-based electrode alloys. The low-temperature performance of $La_{0.75}Mg_{0.25}Ni_{3.5}$ alloy are improved by the addition of $Cu(OH)_2$ to the alkaline electrolyte due to the decomposition of Cu powder to the alloy electrode as recently reported by Shen et al [130].

4.5. Degradation mechanisms

Determining the capacity degradation mechanisms of hydrogen storage alloy electrodes is important for improving their cyclic durability [13]. Systematic investigations have been conducted on the degradation behavior of R–Mg–Ni-based alloy electrodes [51,69–72]. Liao et al. [51] attributed the fast capacity degradation of $La_xMg_{3-x}Ni_9$ alloys to the corrosion of La and Mg, and the large V_H in the hydride phase. Pan et al. [69–72] pointed out that the serious pulverization and oxidation/corrosion of active components during cycling were the two main factors responsible for capacity loss of La–Mg–Ni-based $AB_{3.5}$-type alloys such as $La_{0.7}Mg_{0.3}Ni_{3.4-x}Co_xMn_{0.1}$. The degradation process of $La_{0.7}Mg_{0.3}Ni_{3.4}Mn_{0.1}$ alloy electrode consists of three consecutive stages: particle pulverization and Mg oxidation, Mg and La oxidation and oxidation-passivation (Fig. 8) [69]. Over the initial 5–10 cycles, the alloy particles are pulverized to smaller particles with larger fresh surface areas exposed to the KOH solution. In the meantime, Mg on the alloy surface is oxidized and accordingly a decrease in the amount of active Mg element is apparent. The cooperation of these factors results in a fast activation and capacity loss for La–Mg–Ni-based alloy electrodes. In Mg and La oxidation stage (subsequent 10–30 cycles), a further oxidation/corrosion of active elements such as Mg and La takes place. In this stage, Mg is oxidized first to form a permeable $Mg(OH)_2$ passive layer as a gel-type film because it is the most active element, and it is too loose to prevent the alloy from further oxidation/corrosion. La then separates from the bulk to the alloy surface, and subsequently oxidized to form $La(OH)_3$. In oxidation-passivation stage (after 30 cycles), the oxidation of Mg and La continues with a constant loss of capacity and the oxide layer on the alloy surface grows thicker as cycling continues. A composite surface film of $Mg(OH)_2$ and $La(OH)_3$ decreases the surface reaction kinetics and the diffusivity of hydrogen. Further investigation shows that during electrochemical hydriding/dehydriding, the constituent phases undergo a discrete cell volume expansion between the α- and β-phases, which is the most important reason for the pulverization of alloy particles [70]. The increase in Co content in R–Mg–Ni-based alloys leads to a decrease in the cell volume expansion ratio $\Delta V/V$ of the constituent phases. It prevents alloy pulverization and increases their anti-oxidation/corrosion ability, consequently improving the cycling stability of alloy electrodes [71]. Likewise, the presence of Al decreases alloy pulverization and strengthens anti-oxidation/corrosion property because of the formation of a dense Al oxide film during cycling, which is responsible for the significant improvement in the cycling durability of R–Mg–Ni-based alloys containing Al [72].

5. Conclusions

R–Mg–Ni-based hydrogen storage alloys are a new group of negative electrode materials with high energy density for use in Ni/MH batteries. The introduction of Mg into $AB_{3.0-5.0}$-type rare earth-based hydrogen storage alloys facilitates the formation of a $(La,Mg)Ni_3$ phase with a rhombohedral $PuNi_3$-type structure or a $(La,Mg)_2Ni_7$ phase with a hexagonal Ce_2Ni_7-type structure. These phases possess long-periodic one-dimensional superstructures in which the AB_5 unit ($CaCu_5$-type structure) and the AB_2 unit (Laves structure) are rhombohedrally or hexagonally stacked with a ratio of n:1 along the c-axis direction, consequently resulting in a larger hydrogen storage capacity. The presence of Mg in $LaNi_3$ phase and in La_2Ni_7 phase prevents the amorphization of their hydride phases, leading to a higher electrochemical capacity. As a result, R–Mg–Ni-based hydrogen storage alloys have attracted an increasing amount of attention as next generation negative electrode materials for Ni/MH batteries with high energy density and high power density. For practical applications, numer-

ous efforts to improve the overall electrochemical properties of R–Mg–Ni-based electrode alloys have been undertaken and studies of interest include composition optimization, heat treatment, ball milling treatment, surface treatment, electrolyte modification, operating temperatures and degradation mechanism. Electrode performance was found to depend strongly on the stoichiometric ratio, alloy components and microstructure. The $AB_{3.0}$- and $AB_{3.5}$-type R–Mg–Ni-based alloys exhibit a higher discharge capacity and better electrochemical kinetics. The specific function of the constituent elements including Mg, Ce, Pr, Nd, Co, Mn, Al, Zr, W, Fe, Cu and Cr are discussed. Optimum compositions contain mainly metallic elements of La, Mg, Ni, Co, Mn and Al. Annealing treatment significantly increased the discharge capacity, improves the cyclic stability and enhances the high rate dischargeability. The optimized annealing temperature lies between 850 and 950 °C. Mechanistic investigations indicate that the pulverization of alloy particles and the oxidation/corrosion of active components during cycling are the two main factors responsible for the fast capacity degradation of R–Mg–Ni-based alloy electrodes, and the degradation progress is divided into three consecutive stages including pulverization and Mg oxidation, Mg and La oxidation, and oxidation-passivation. Consequently, a decrease in the pulverization of the alloy particles and an increase in their anti-oxidation/corrosion ability are necessary for an improvement in cyclic stability. Co and Al produce these effects in R–Mg–Ni-based electrode alloys. Despite the overall electrochemical properties of R–Mg–Ni-based electrode alloys being significantly improved over the last decade, their practical application is still a challenge because of the industrialized preparation techniques and the cost of alloys. Therefore, optimized preparation techniques for industrial scale and low-cost R–Mg–Ni-based electrode alloys (low-Co or Co-free) with a high discharge capacity, a long cycle life and good kinetics are still needed to satisfy the requirements for Ni/MH batteries.

Author contributions

Y.F.L. and HG.P. designed topic; Y.F.L., Y.H.C., L.H., and M.X.G. collected literatures, and Y.F.L. and H.G.P. wrote the paper.

Acknowledgments

The authors would like to acknowledge the financial supports from National Nature Science Foundation of China (50701040 and 50631020), from Ministry of Science and Technology of China (2009AA05Z106 and 2010CB631304) and from National Nature Science Foundation for Distinguished Young Scholars of China (51025102).

References

[1] M.S. Dresselhaus, I.L. Thomas, Nature 414 (2001) 332–337.
[2] M. Winter, R.J. Brodd, Chem. Rev. 104 (2004) 4245–4269.
[3] M.S. Whittingham, Chem. Rev. 104 (2004) 4271–4301.
[4] J. Kleperis, G. WóJcik, A. Czerwinski, J. Skowronski, M. Kopczyk, M. Beltowska-Brzezinska, J. Solid State Electrochem. 5 (2001) 229–249.
[5] V. Pop, H.J. Bergveld, P.H.L. Notten, P.P.L. Regtien, Meas. Sci. Technol. 16 (2005) R93–R110.
[6] J.J.G. Willems, Philips J. Res. 39 (Suppl. 1) (1984) 1–94.
[7] J.O. Besenhard, Handbook of Battery Materials, 1st ed., Wiley–VCH, New York, 1999.
[8] J.H.N. Van Vucht, F.A. Kuijpers, H.C.A.M. Bruning, Philips Res. Rep. 25 (1970) 133–140.
[9] P.A. Boter, Rechargeable electrochemical cell, US Patent 4,004,943.
[10] N. Furukawa, T. Ueda, Sanyo NiMH batteries outperform Li–ion Nikkei Electronics Asia, 1996, pp. 80–83.
[11] L. Gaines, M. Wang, Science 269 (1995) 742–743.
[12] A. Ledovskikh, E. Verbitskiy, A. Ayeb, P.H.L. Notten, J. Alloys Compd. 356–357 (2003) 742–745.
[13] F. Feng, M. Geng, D.O. Northwood, Int. J. Hydrogen Energy 26 (2001) 725–734.
[14] H. Ye, H. Zhang, Adv. Eng. Mater. 3 (2001) 481–485.
[15] F. Cuevas, J.–M. Joubert, M. Latroche, A. Percheron-Guégan, Appl. Phys. A 72 (2001) 225–238.
[16] J.J. Reilly, G.D. Adzic, J.R. Johnson, T. Vogt, S. Mukerjee, J. McBreen, J. Alloys Compd. 293–295 (1999) 569–582.
[17] H. Ewe, E.W. Justi, K. Stephan, Energy Convers. 13 (1973) 109–113.
[18] T. Sakai, T. Hazama, H. Miyamura, N. Kuriyama, A. Kato, H. Ishikawa, J. Less Common Met. 172–174 (1991) 1175–1184.
[19] H.G. Pan, J.X. Ma, C.S. Wang, S.A. Chen, X.H. Wang, C.P. Chen, Q.D. Wang, J. Alloys Compd. 293–295 (1999) 648–652.
[20] Y.Q. Lei, S.K. Zhang, G.L. Lü, L.X. Chen, Q.D. Wang, F. Wu, J. Alloys Compd. 330–332 (2002) 861–865.
[21] S. Bliznakov, E. Lefterova, N. Dimitrov, K. Petrov, A. Popov, J. Power Sources 176 (2008) 381–386.
[22] K. Kadir, T. Sakai, I. Uehara, J. Alloys Compd. 257 (1997) 115–121.
[23] K. Kadir, N. Kuriyama, T. Sakai, I. Uehara, L. Eriksson, J. Alloys Compd. 284 (1999) 145–154.
[24] K. Kadir, T. Sakai, I. Uehara, J. Alloys Compd. 287 (1999) 264–270.
[25] K. Kadir, T. Sakai, I. Uehara, J. Alloys Compd. 302 (2000) 112–117.
[26] J. Chen, H.T. Takeshita, H. Tanaka, N. Kuriyama, T. Sakai, I. Uehara, M. Haruta, J. Alloys Compd. 302 (2000) 304–313.
[27] J. Chen, N. Kuriyama, H.T. Takeshita, H. Tanaka, T. Sakai, M. Haruta, Electrochem. Solid-State Lett. 3 (2000) 249–252.
[28] T. Kohno, H. Yoshida, F. Kawashima, T. Inaba, I. Sakai, M. Yamanoto, M. Kands, J. Alloys Compd. 311 (2000) L5–L7.
[29] H.G. Pan, Y.F. Liu, M.X. Gao, Y.Q. Lei, Q.D. Wang, J. Electrochem. Soc. 150 (2003) A565–A570.
[30] B. Liao, Y.Q. Lei, G.L. Lu, L.X. Chen, H.G. Pan, Q.D. Wang, J. Alloys Compd. 356–357 (2003) 746–749.
[31] S.R. Ovshinsky, M.A. Fetcenko, J. Ross, Science 260 (1993) 176–181.
[32] D.M. Kim, K.J. Jang, J.Y. Lee, J. Alloys Compd. 293–295 (1999) 762–769.
[33] Y.L. Du, X.G. Yang, Q.A. Zhang, Y.Q. Lei, M.S. Zhang, Int. J. Hydrogen Energy 26 (2001) 333–337.
[34] S.K. Dhar, M.A. Fetcenko, S.R. Ovshinsky, IEEE 0-7803-6545-3 (2001) 325–336.
[35] R. Parimala, M.V. Ananth, S. Ramaprabhu, M. Raju, Int. J. Hydrogen Energy 29 (2004) 509–513.
[36] M. Kandavel, V.V. Bhat, A. Rougier, L. Aymard, G.-A. Nazri, J.-M. Tarascona, Int. J. Hydrogen Energy 33 (2008) 3754–3761.
[37] Y.Q. Lei, Y.M. Wu, M. Yang, J. Wu, Q.D. Wang, Z. Phys. Chem. 183 (1994) 379–384.
[38] D.L. Sun, Y.Q. Lei, W.H. Liu, J.J. Jiang, J. Wu, Q.D. Wang, J. Alloys Compd. 231 (1995) 621–624.
[39] H. Inoue, S. Hazuia, S. Nohara, C. Iwakura, Electrochim. Acta 43 (1998) 2221–2224.
[40] Y. Zhang, Y.Q. Lei, L.X. Chen, J. Yuan, Z.H. Zhang, Q.D. Wang, J. Alloys Compd. 337 (2002) 296–302.
[41] C. Rongeat, M.H. Grosjean, S. Ruggeri, M. Dehmas, S. Bourlot, S. Marcotte, L. Roué, J. Power Sources 158 (2006) 747–753.
[42] G. He, L.F. Jiao, H.T. Yuan, Y.Y. Zhang, Y.J. Wang, J. Alloys Compd. 450 (2008) 375–379.
[43] M. Tsukahara, K. Takahashi, T. Mishima, T. Sakai, H. Miyamura, N. Kuriyama, J. Uehara, J. Alloys Compd. 226 (1995) 203–207.
[44] H.G. Pan, Y.F. Zhu, M.X. Gao, Q.D. Wang, J. Electrochem. Soc. 149 (2002) A829–A833.
[45] Y.F. Zhu, H.G. Pan, M.X. Gao, J.X. Ma, S.Q. Li, Q.D. Wang, Int. J. Hydrogen Energy 27 (2002) 287–293.
[46] H.G. Pan, Y.F. Zhu, M.X. Gao, Y.F. Liu, R. Li, Y.Q. Lei, Q.D. Wang, J. Alloys Compd. 370 (2004) 254–260.
[47] X.B. Yu, G.S. Walker, D.M. Grant, Appl. Phys. Lett. 87 (2005) 133121.
[48] X.B. Yu, Z.X. Yang, S.L. Feng, Z. Wu, N.X. Xu, Int. J. Hydrogen Energy 31 (2006) 1176–1181.
[49] Y.F. Liu, H.G. Pan, M.X. Gao, R. Li, Q.D. Wang, J. Phys. Chem. C 112 (2008) 16682–16690.
[50] Y.F. Liu, S.S. Zhang, R. Li, M.X. Gao, K. Zhong, H. Miao, H.G. Pan, Int. J. Hydrogen Energy 33 (2008) 728–734.
[51] B. Liao, Y.Q. Lei, L.X. Chen, G.L. Lu, H.G. Pan, Q.D. Wang, J. Power Sources 129 (2004) 358–367.
[52] B. Liao, Y.Q. Lei, L.X. Chen, G.L. Lu, H.G. Pan, Q.D. Wang, J. Alloys Compd. 376 (2004) 186–195.
[53] B. Liao, Y.Q. Lei, L.X. Chen, G.L. Lu, H.G. Pan, Q.D. Wang, Electrochim. Acta 50 (2004) 1057–1063.
[54] B. Liao, Y.Q. Lei, L.X. Chen, G.L. Lu, H.G. Pan, Q.D. Wang, J. Alloys Compd. 404–406 (2005) 665–668.
[55] B. Liao, Y.Q. Lei, L.X. Chen, G.L. Lu, H.G. Pan, Q.D. Wang, J. Alloys Compd. 415 (2006) 239–243.
[56] R.V. Denys, B. Riabov, V.A. Yartys, R.G. Delaplane, M. Sato, J. Alloys Compd. 446–447 (2007) 166–172.
[57] H. Oesterreicher, H. Bittner, J. Less-Common Met. 73 (1980) 339–344.
[58] H.G. Pan, Y.F. Liu, M.X. Gao, Y.F. Zhu, Y.Q. Lei, Q.D. Wang, J. Alloys Compd. 351 (2003) 228–234.
[59] H.G. Pan, Y.F. Liu, M.X. Gao, Y.F. Zhu, Y.Q. Lei, Q.D. Wang, J. Electrochem. Soc. 151 (2004) A374–A380.
[60] Y.F. Liu, H.G. Pan, M.X. Gao, Y.F. Zhu, Y.Q. Lei, Mater. Sci. Eng. A 372 (2004) 163–172.

[61] H.G. Pan, Y.F. Liu, M.X. Gao, Y.F. Zhu, Y.Q. Lei, Q.D. Wang, Mater. Chem. Phys. 84 (2004) 171–181.
[62] Y.F. Liu, H.G. Pan, M.X. Gao, Y.F. Zhu, Y.Q. Lei, Q.D. Wang, Int. J. Hydrogen Energy 29 (2004) 297–305.
[63] Y.F. Liu, H.G. Pan, M.X. Gao, Y.F. Zhu, Y.Q. Lei, J. Alloys Compd. 365 (2004) 246–252.
[64] Y.F. Liu, H.G. Pan, M.X. Gao, R. Li, Y.Q. Lei, J. Alloys Compd. 376 (2004) 296–303.
[65] Y.F. Liu, H.G. Pan, M.X. Gao, R. Li, Y.Q. Lei, J. Alloys Compd. 376 (2004) 304–313.
[66] H.G. Pan, Q.W. Jin, M.X. Gao, Y.F. Liu, R. Li, G.L. Lu, Y.Q. Lei, J. Alloys Compd. 373 (2004) 237–245.
[67] H.G. Pan, Y.F. Liu, M.X. Gao, Y.Q. Lei, Q.D. Wang, J. Electrochem. Soc. 152 (2005) A326–A332.
[68] Y.F. Liu, H.G. Pan, M.X. Gao, Y.F. Zhu, Y.Q. Lei, Q.D. Wang, Electrochim. Acta 49 (2004) 545–555.
[69] Y.F. Liu, H.G. Pan, M.X. Gao, Y.Q. Lei, Q.D. Wang, J. Electrochem. Soc. 152 (2005) A1089–A1095.
[70] Y.F. Liu, H.G. Pan, M.X. Gao, Y.Q. Lei, Q.D. Wang, J. Alloys Compd. 403 (2005) 296–304.
[71] Y.F. Liu, H.G. Pan, Y.J. Yue, X.F. Wu, N. Chen, Y.Q. Lei, J. Alloys Compd. 395 (2005) 291–299.
[72] Y.F. Liu, H.G. Pan, M.X. Gao, H. Miao, Y.Q. Lei, Q.D. Wang, Int. J. Hydrogen Energy 33 (2008) 124–133.
[73] H.G. Pan, N. Chen, M.X. Gao, R. Li, Y.Q. Lei, Q.D. Wang, J. Alloys Compd. 397 (2005) 306–312.
[74] H.G. Pan, Y.J. Yue, M.X. Gao, X.F. Wu, N. Chen, Y.Q. Lei, Q.D. Wang, J. Alloys Compd. 397 (2005) 269–275.
[75] H.G. Pan, X.F. Wu, M.X. Gao, N. Chen, Y.J. Yue, Y.Q. Lei, Int. J. Hydrogen Energy 31 (2006) 517–523.
[76] H.G. Pan, S. Ma, J. Shen, J.J. Tian, J.L. Deng, M.X. Gao, Int. J. Hydrogen Energy 32 (2007) 2949–2956.
[77] H. Miao, Y.F. Liu, Y. Lin, D. Zhu, L. Jiang, H.G. Pan, Int. J. Hydrogen Energy 33 (2008) 134–140.
[78] S. Ma, M.X. Gao, R. Li, H.G. Pan, Y.Q. Lei, J. Alloys Compd. 457 (2008) 457–464.
[79] R. Tang, Z.H. Zhang, L.Q. Liu, Y.N. Liu, J.W. Zhu, G. Yu, Int. J. Hydrogen Energy 29 (2004) 851–858.
[80] T. Ozaki, M. Kanemoto, T. Kakeya, Y. Kitano, M. Kuzuhara, M. Watada, S. Tanase, T. Sakai, J. Alloys Compd. 446–447 (2007) 620–624.
[81] L.F. Cheng, R.B. Wang, Z.H. Pu, Z.L. Li, D.N. He, B.J. Xia, J. Power Sources 185 (2008) 1519–1523.
[82] X.P. Dong, F.X. Lü, Y.H. Zhang, L.Y. Yang, X.L. Wang, Mater. Chem. Phys. 108 (2008) 251–256.
[83] R. Tang, Y.N. Liu, C.C. Zhu, J.W. Zhu, G. Yu, Mater. Chem. Phys. 95 (2006) 130–134.
[84] D.J. Cuscueta, M. Melnichuk, H.A. Peretti, H.R. Salva, A.A. Ghilarducci, Int. J. Hydrogen Energy 33 (2008) 3566–3570.
[85] Y. Li, S.M. Han, J.H. Li, X.L. Zhu, L. Hu, J. Alloys Compd. 458 (2008) 357–362.
[86] J. Guo, W.Q. Jiang, R.J. Xiao, C.K. Huang, D. Huang, J. Alloys Compd. 390 (2005) 301–304.
[87] R. Tang, Y.N. Liu, C.C. Zhu, J.W. Zhu, G. Yu, Intermetallics 14 (2006) 361–366.
[88] F.L. Zhang, Y.C. Luo, K. Sun, D.H. Wang, R.X. Yan, L. Kang, J.H. Chen, J. Alloys Compd. 424 (2006) 218–224.
[89] X.L. Zhao, Y.H. Zhang, B.W. Li, H.P. Ren, X.P. Dong, X.L. Wang, J. Alloys Compd. 454 (2008) 437–441.
[90] P. Zhang, Y.N. Liu, J.W. Zhu, X.D. Wei, G. Yu, Int. J. Hydrogen Energy 32 (2007) 2488–2493.
[91] H.L. Chu, Y. Zhang, S.J. Qiu, Y.N. Qi, L.X. Sun, F. Xu, Q. Wang, C. Dong, J. Alloys Compd. 457 (2008) 90–96.
[92] Y.H. Zhang, X.P. Dong, B.W. Li, H.P. Ren, Z.W. Wu, X.L. Wang, J. Alloys Compd. 465 (2008) 422–428.
[93] L.L. Xiao, Y.J. Wang, Y. Liu, D.W. Song, L.F. Jiao, H.T. Yuan, Int. J. Hydrogen Energy 33 (2008) 3925–3929.
[94] X.B. Zhang, D.Z. Sun, W.Y. Yin, Y.J. Chai, M.S. Zhao, Electrochim. Acta 50 (2005) 1957–1964.
[95] X.B. Zhang, D.Z. Sun, W.Y. Yin, Y.J. Chai, M.S. Zhao, J. Power Sources 154 (2006) 290–297.
[96] X.B. Zhang, D.Z. Sun, W.Y. Yin, Y.J. Chai, M.S. Zhao, Electrochim. Acta 50 (2005) 2911–2918.
[97] S.Q. Shi, C.R. Li, W.H. Tang, J. Alloys Compd. 476 (2009) 874–877.
[98] Y.H. Zhang, X.P. Dong, G.Q. Wang, S.H. Guo, J.Y. Ren, X.L. Wang, Int. J. Hydrogen Energy 32 (2007) 594–599.
[99] X.L. Wang, Y.H. Zhang, D.L. Zhao, X.P. Dong, S.H. Guo, G.Q. Wang, J. Alloys Compd. 446–447 (2007) 625–629.
[100] Y.H. Zhang, D.L. Zhao, H.P. Ren, Z.W. Wu, X.P. Dong, X.L. Wang, J. Alloys Compd. 446–447 (2007) 643–647.
[101] Y.H. Zhang, B.W. Li, H.P. Ren, Z.W. Wu, X.P. Dong, X.L. Wang, J. Alloys Compd. 460 (2008) 414–420.
[102] Y.H. Zhang, B.W. Li, H.P. Ren, Y. Cai, X.P. Dong, X.L. Wang, Int. J. Hydrogen Energy 32 (2007) 3420–3426.
[103] Y.H. Zhang, B.W. Li, H.P. Ren, Z.W. Wu, X.P. Dong, X.L. Wang, J. Alloys Compd. 461 (2008) 591–597.
[104] X.P. Dong, F.X. Lü, L.Y. Yang, Y.H. Zhang, X.L. Wang, Mater. Chem. Phys. 112 (2008) 596–602.
[105] T.Z. Si, Q.A. Zhang, N. Liu, Int. J. Hydrogen Energy 33 (2008) 1729–1734.
[106] M. Zhu, C.H. Peng, L.Z. Ouyang, Y.Q. Tong, J. Alloys Compd. 426 (2006) 316–321.
[107] H.L. Chu, S.J. Qiu, L.X. Sun, Y. Zhang, F. Xu, T. Jiang, W.X. Li, M. Zhu, W.Y. Hu, Electrochim. Acta 52 (2007) 6700–6706.
[108] Y.N. Qi, F. Xu, H.L. Chu, L.X. Sun, T. Jiang, M. Zhu, Int. J. Hydrogen Energy 32 (2007) 4894–4899.
[109] H.L. Chu, S.J. Qiu, L.X. Sun, Y. Zhang, F. Xu, M. Zhu, W.Y. Hu, Int. J. Hydrogen Energy 33 (2008) 755–761.
[110] D.R. Lide, CRC Handbook of Chemistry and Physics, 89th ed., CRC Press/Taylor and Francis, Boca Raton, FL, 2009 (Internet Version 2009).
[111] E. Akiba, H. Hayakawa, T. Kohno, J. Alloys Compd. 408–412 (2006) 280–283.
[112] F. Li, K. Young, T. Ouchi, M.A. Fetcenko, J. Alloys Compd. 471 (2009) 371–377.
[113] C.H. Peng, M. Zhu, J. Alloys Compd. 375 (2004) 324–329.
[114] F.L. Zhang, Y.C. Luo, D.H. Wang, R.X. Yan, L. Kang, J.H. Chen, J. Alloys Compd. 439 (2007) 181–188.
[115] S. Yasuoka, Y. Magari, T. Murata, T. Tanaka, J. Ishida, H. Nakamura, T. Nohma, M. Kihara, Y. Baba, H. Teraoka, J. Power Sources 156 (2006) 662–666.
[116] D.H. Wang, Y.C. Luo, R.X. Yan, F.L. Zhang, L. Kang, J. Alloys Compd. 413 (2006) 193–197.
[117] Y.H. Zhang, D.L. Zhao, B.W. Li, X.L. Zhao, Z.W. Wu, X.L. Wang, Int. J. Hydrogen Energy 33 (2008) 1868–1875.
[118] B.W. Li, H.P. Ren, Y.H. Zhang, X.P. Dong, J.Y. Ren, X.L. Wang, J. Alloys Compd. 425 (2006) 399–405.
[119] H.G. Pan, Y.F. Liu, M.X. Gao, Y.F. Zhu, Y.Q. Lei, Q.D. Wang, Int. J. Hydrogen Energy 28 (2003) 113–117.
[120] Y.F. Liu, Q.W. Jin, M.X. Gao, Y.F. Zhu, Z.H. Zhang, H.G. Pan, Rare Metal Mater. Eng. 32 (2003) 942–945.
[121] Y.F. Liu, H.G. Pan, M.X. Gao, Y.F. Zhu, Y.Q. Lei, Trans. Nonferrous Met. Soc. China 13 (2003) 25–28.
[122] D.W. Song, Y.J. Wang, Y. Liu, S.M. Han, L.F. Jiao, H.T. Yuan, J. Rare Earths 26 (2008) 398–401.
[123] A. Percheron-Guegan, J.M. Welter, in: L. Schlapbach (Ed.), Hydrogen in Intermetallic Compounds I, Springer Verlag, New York, 1988, p. 28.
[124] D.H. Wang, Y.C. Luo, R.X. Yan, L. Kang, X.G. Hou, Trans. Nonferrous Met. Soc. China 17 (2007) s972–s977.
[125] Y.H. Zhang, B.W. Li, H.P. Ren, S.H. Guo, Q. Yan, X.L. Wang, J. Alloys Compd. 485 (2009) 333–339.
[126] Z.W. Dong, Y.M. Wu, L.Q. Ma, X.D. Shen, L.M. Wang, Mater. Res. Bull. 45 (2010) 256–261.
[127] L. Jiang, G.X. Li, L.Q. Xu, W.Q. Jiang, Z.Q. Lan, J. Guo, Int. J. Hydrogen Energy 35 (2010) 204–209.
[128] X.J. Zhao, Q. Li, K.C. Chou, H. Liu, G.W. Lin, J. Alloys Compd. 473 (2009) 428–432.
[129] Y.H. Zhang, B.W. Rafi-ud-din, H.P. Li, S.H. Ren, X.L. Guo, Wang, Mater. Charact. 61 (2010) 305–311.
[130] X.Q. Shen, Y.G. Chen, M.D. Tao, C.L. Wu, G. Deng, Electrochim. Acta 54 (2009) 2581–2587.
[131] D. Linden, Handbook of Batteries, 2nd ed., McGrawHill, New York, 1995.